

1 Article

## 2 Design and realization of a Bidirectional Full Bridge 3 Converter with improved modulation strategies

4 Filippo Pellitteri<sup>1,\*</sup>, Rosario Miceli<sup>1</sup>, Giuseppe Schettino<sup>1</sup>, Fabio Viola<sup>1</sup> and Luigi Schirone<sup>2</sup>

5 <sup>1</sup> Department of Engineering, University of Palermo; rosario.miceli@unipa.it; giuseppe.schettino@unipa.it;  
6 fabio.viola.unipa.it

7 <sup>2</sup> School of Aerospace Engineering, Sapienza University of Rome; luigi.schirone@uniroma1.it

8 \* Correspondence: filippo.pellitteri@unipa.it

9 **Abstract:** In this paper a Full-Bridge Converter (FBC) for bidirectional power transfer is presented.  
10 The proposed FBC is an isolated DC-DC bidirectional converter, connected to a double voltage  
11 source: a voltage bus on one side and a Stack Of Super-Capacitors (SOSC) on the other side. The  
12 control law aims at the regulation either of the bus current (when the load requires power) or of the  
13 SOSC current (when the stack requires a recharge). Analysis and design of the proposed FBC are  
14 discussed. A Phase Shift Modulation (PSM) scheme is proposed, along with an improved  
15 modulation variant for the efficiency optimization, through a proper reduction of the transformer  
16 power losses. The realized prototype, compliant with automotive applications, is presented and  
17 experimental results are highlighted. The target power level is 2 kW.

18 **Keywords:** full-bridge converter; phase shift modulation; supercapacitors; isolated DC-DC  
19 bidirectional converter

20

### 21 1. Introduction

22 Energy Storage Systems allow to durably collect the electrical energy arising from different  
23 sources. With respect to the electrical grid, alternative ways of obtaining power are renewable  
24 sources and energy harvesting [1-3]. As far as storage systems are concerned, their hybridization is  
25 gathering momentum in several fields, such as automotive or aerospace, due to the opportunity to  
26 integrate different features in the same storage system. Among the possible electrical storage  
27 elements, batteries and supercapacitors offer significant benefits in terms of energy density and  
28 power density respectively, so that their combination can lead to improvements in terms of total cost  
29 and efficiency [4-9]. Investigation on possible power system architectures and power converter  
30 topologies in order to properly manage the electrical energy inside a hybrid storage system is  
31 therefore an attractive research topic [10-12].

32 According to specific application and power level, different types of power system  
33 architectures are possible. A common DC voltage bus is generally used to supply the existing loads,  
34 and this bus could be either directly connected to a battery or connected to it through a DC-DC  
35 converter. The supercapacitor instead shall be properly managed in order to supply the load or to  
36 recharge the battery itself: a bidirectional DC-DC converter can be used for this purpose. The  
37 mentioned DC-DC bidirectional converter shall be able to control the charge/discharge of the  
38 supercapacitor from/to the bus.

39 State of art and future trends concerning DC-DC converters for automotive applications are  
40 widely provided in [13], whereas different investigations on DC-DC bidirectional converters for  
41 both supercapacitors and battery charging applications are provided in [14-17], with particular focus  
42 on reliability, ease of control, sizing and robustness. Due to the potentially high voltage range of a  
43 stack of supercapacitors, proper DC-DC converter architectures could be used: in [18-21]  
44 high-voltage-ratio topologies are described, feasible for several applications such as automotive, DC  
45 microgrids and renewable energy sources. At the same time, such high voltage levels could suggest

46 the use of galvanic isolation in order to guarantee safety: in [22-27] different applications of isolated  
47 DC-DC converters for energy storage management are reported.

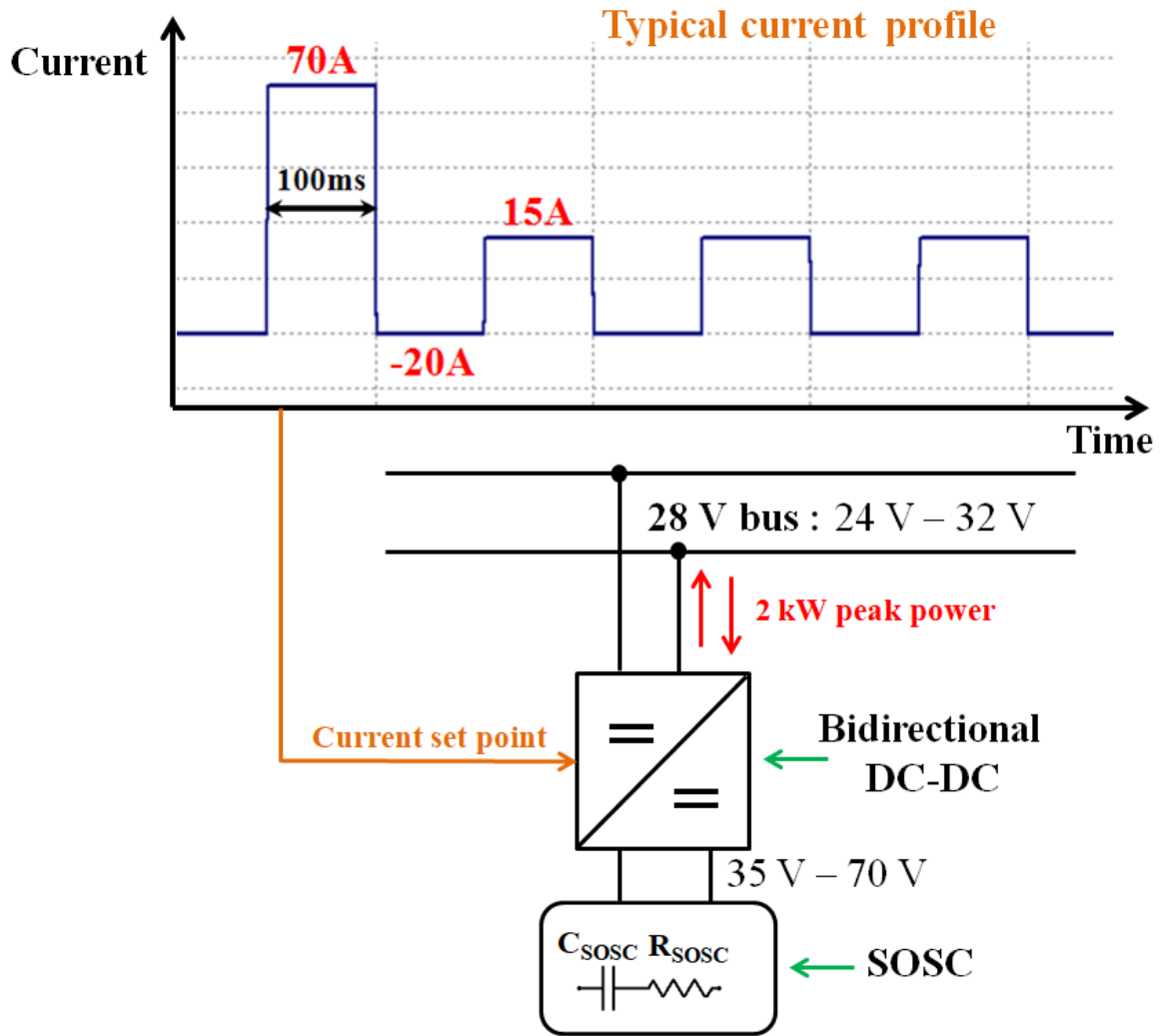
48 In this paper, an insulated DC-DC bidirectional converter is proposed for the management of a  
49 hybrid storage system based on battery and supercapacitor. The proposed topology is a full-bridge  
50 converter (FBC), which has been realized and experimentally tested with two DC sources emulating  
51 a Stack Of Supercapacitors (SOSC) whose maximum voltage is 70 V and a 28 V bus. The rated power  
52 level is 2 kW.

53 The proposed power converter could find its application whenever a battery-supercapacitor  
54 hybrid storage system is present: the battery provides average power, whereas the supercapacitance  
55 is able to provide the peak power pulses. Typical application examples of power system  
56 architectures are those inside an Electric Vehicle (EV), based on an automotive DC voltage bus, or  
57 inside a space launcher, based on an avionic DC voltage bus.

58 This paper is organized as follows: Section 2 provides a description of the proposed power  
59 system architecture and analyzes the proposed bidirectional DC-DC converter; Section 3 focuses on  
60 the Full Bridge converter design, accordingly comparing different modulation strategies; Section 4  
61 reports experimental results concerning a Full Bridge converter prototype, able to transfer a 2kW  
62 power; in Section 5 conclusions are given.

## 63 2. Analysis of the Full Bridge Converter (FBC)

64 The aim of the proposed DC-DC converter is to manage the energy flow between two energy  
65 sources, being in the specific case a Stack Of Supercapacitors (SOSC) and a DC voltage bus, as  
66 highlighted in Figure 1, showing the power system architecture. A typical current profile, required  
67 from the bus section, is highlighted as well: the positive current values correspond to a SOSC  
68 discharge, whereas the negative ones correspond to a SOSC recharge. The maximum required  
69 current value is 70 A, which is equivalent to a maximum rated power of 2 kW.



70  
71 **Figure 1.** Power system architecture.

72 *2.1. Energy sources model*

73 The SOSC voltage lies in the range 35 V – 70 V, whereas the nominal DC bus voltage is 28 V. In  
74 Table 1 the SOSC parameters and voltage range are reported, where  $C_{sosc}$  and  $R_{sosc}$  are the SOSC  
75 equivalent capacitance and resistance.

76 **Table 1.** SOSC parameters and voltage range.

$C_{sosc}$	$R_{sosc}$	$V_{min}$	$V_{max}$
10 F	70 mΩ	35 V	70 V

77  
78 Being equal to the product between  $C_{sosc}$  and  $R_{sosc}$ , the SOSC charge/discharge time constant is  
79 equivalent to hundreds of ms, so that the SOSC can be considered as a DC power source with respect to a  
80 converter switching frequency in the order of tens-of-kHz. For this reason the proposed converter can be  
81 analyzed and designed as an actual DC-DC converter.

82 In Table 2 the DC bus specifications concerning the voltage level are reported.

83 **Table 2.** DC bus voltage minimum, nominal and maximum level.

$V_{min}$	$V_{nom}$	$V_{maz}$
24 V	28 V	32 V

84 2.2. Full Bridge Converter analysis

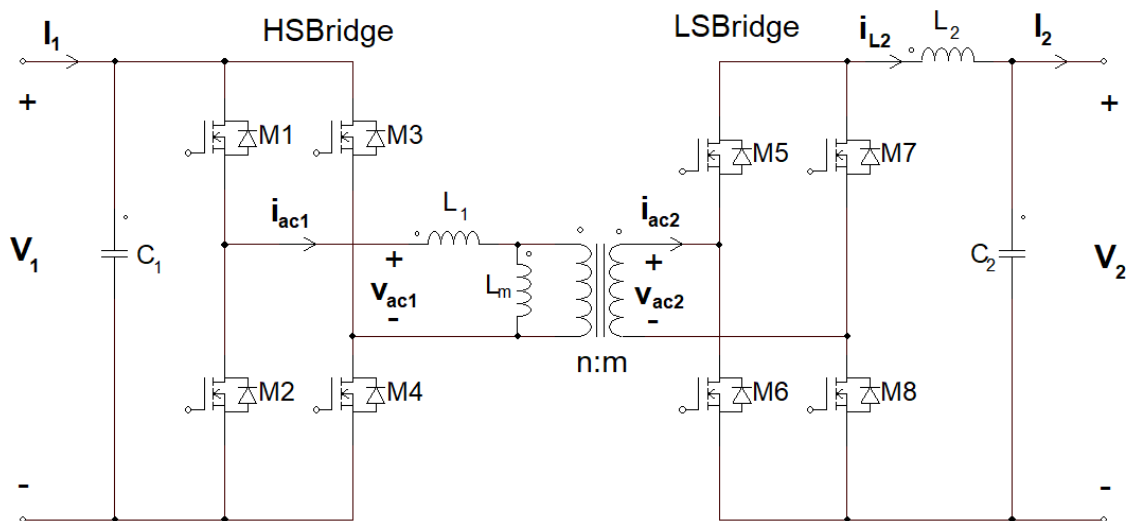
85 In Figure 2 the schematic of the proposed Full Bridge Converter (FBC) is shown. The FBC is an  
 86 insulated topology, featuring a transformer between the sections connected to the DC voltages  $V_1$   
 87 and  $V_2$ , representing the SOSOC and the bus respectively. As far as the transformer is concerned,  $L_1$   
 88 and  $L_m$  are the equivalent primary leakage and magnetizing inductances respectively, whereas  $n:m$   
 89 is the turns ratio. Each of the H-bridges in the primary and in the secondary side of the transformer  
 90 consists of four bi-directional switches, in this specific case four enhancement n-channel MOSFETs:  
 91 the primary side H-bridge consists of M1-M2-M3-M4, whereas the secondary side one consists of  
 92 M5-M6-M7-M8. In this network therefore energy can flow in both directions, either from  $V_1$  to  $V_2$   
 93 from  $V_2$  to  $V_1$ : in the first case the primary H-bridge acts as an inverter and the secondary one as a  
 94 rectifier, in the second case the H-bridges play the opposite roles.

95 As far as the DC voltages at the primary and at the secondary section are concerned, referenced  
 96 as  $V_1$  and  $V_2$  respectively, the proposed converter implements a step-down operation, so that it can  
 97 be considered as an insulated buck converter.

98 The primary and secondary H-bridges can be therefore referenced as High-Side Bridge  
 99 (HSBridge) and Low-Side Bridge (LSBridge).

100  $L_2$  is the converter inductor, placed in series with the LSBridge.

101



102

103 **Figure 2.** Schematic of the Full Bridge Converter.

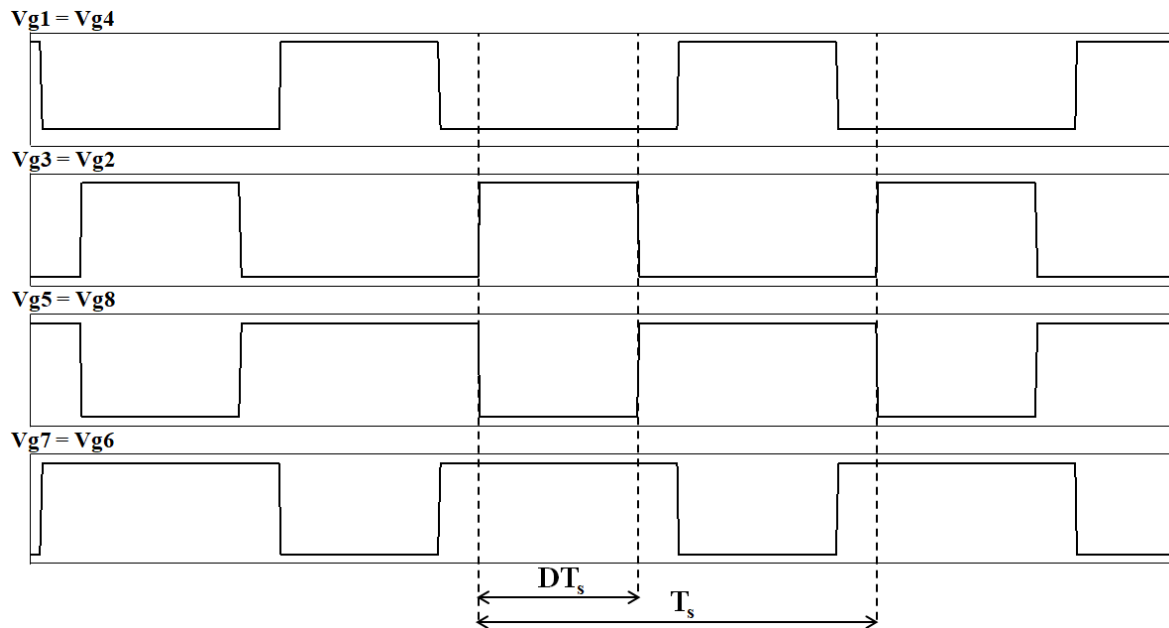
104 2.3. Possible modulation techniques

105 Two possible modulation schemes have been investigated on the proposed FBC, as shown in  
 106 Figure 3 and 4, being  $V_{gn}$  the logic level applied to the gate-source voltage of the MOSFET  $M_n$ : the  
 107 Pulse Width Modulation (PWM) and the Phase Shift Modulation (PSM).

108 Figure 3 shows the PWM scheme: M1 and M4 gate signals are in phase, as well as M2 and M3  
 109 gate signals, and a phase difference occurs between the diagonals M1-M4 and M2-M3; the  
 110 secondary-side gate signals are obtained by logical negation (NOT) of the primary-side signals, as  
 111 highlighted in the figure. The on-time of each HSBridge switch is  $DT_s$ , where  $D$  is the duty-cycle and  
 112  $T_s$  the switching period, being the duty-cycle limited to less than 50% in order to avoid short-circuit  
 113 at the primary side.

114

115

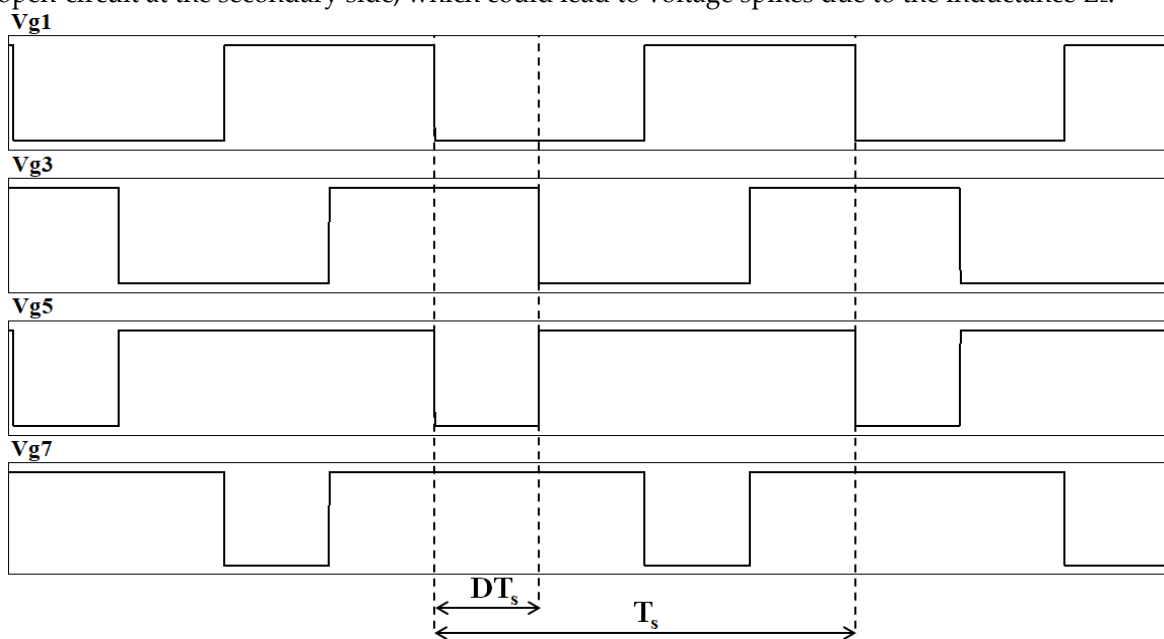


116  
117

**Figure 3.** Gate signals in the PWM case.

118 Figure 4 shows the PSM scheme: M1 and M2 are always in phase opposition, as well as M3 and  
119 M4; a phase difference, corresponding to the duty-cycle  $D$ , occurs between them. The PWM,  
120 therefore, is converted into a phase shift modulation.

121 At the same way as in the PWM, the duty-cycle  $D$  is limited to less than 50% in order to avoid  
122 open-circuit at the secondary side, which could lead to voltage spikes due to the inductance  $L_2$ .



123  
124

**Figure 4.** Gate signals in the PSM case.

125 The PSM scheme has been preferred to the PWM, since the PWM scheme involves higher  
126 power losses, due to the time windows, inside each switching period, when all the four HSBridge  
127 MOSFETs (M1-M2-M3-M4) are in open state, thus forcing current in the parallel-connected diodes.

128 The proposed converter aims at the regulation of the power in terms of both amount and  
129 direction.

130 Considering that  $V_1$  and  $V_2$  are two DC voltage sources – a Stack Of Supercapacitors and a DC  
131 bus respectively - the power regulation is therefore consisting in a current regulation.

132 **3. Design and modulation strategies for the proposed converter**

133 3.1. *Choice of the n:m transformer ratio*

134 In a conventional full-bridge converter, with a resistive load at its output, the ratio of the output  
 135 voltage  $V_2$  to the input voltage  $V_1$  is equal to:

$$\frac{V_2}{V_1} = \frac{2mD}{n} \tag{1}$$

136 This means that for the designed power converter, where voltage sources are applied at both  
 137 ports (the  $V_1$  SOSC source at the input and the  $V_2$  bus source at the output), this condition  
 138 corresponds to a “current balance”, meaning that no DC current is flowing.

139 In order to produce a current flow, this condition shall be modified. If the SOSC has to  
 140 discharge into the bus, the duty-cycle, representing the control parameter, shall be increased  
 141 towards the maximum limit, i.e.  $D = 0.5$ .

142 The most critical condition is represented by the minimum voltage difference between SOSC  
 143 and bus, that is when the SOSC is at its minimum voltage ( $V_1 = 35V$ ) and the bus is at its maximum  
 144 voltage ( $V_2 = 32V$ ). In this condition, the  $V_2$ -to- $V_1$  ratio is at its maximum value, so that, considering  
 145 that  $D$  must be less than 0.5, the secondary-to-primary ratio  $m:n$  shall be higher than 1 according to  
 146 (1), especially considering the case of a positive bus current  $I_2$ . For this reason, the selected  $n$  and  $m$   
 147 have been chosen according to the following ratio:

$$n : m = 2 : 3 \tag{2}$$

148 A higher-than-1 turns ratio is even more required considering the voltage drop in the primary  
 149 side, due to the  $R_{SOSC}$ , possibly leading the voltage  $V_1$  from 35 V to less than 32 V.

150 If the leakage inductance effect is neglected, the  $L_2$  average current  $I_{L2,av}$ , corresponding to the  
 151 bus current, is the following:

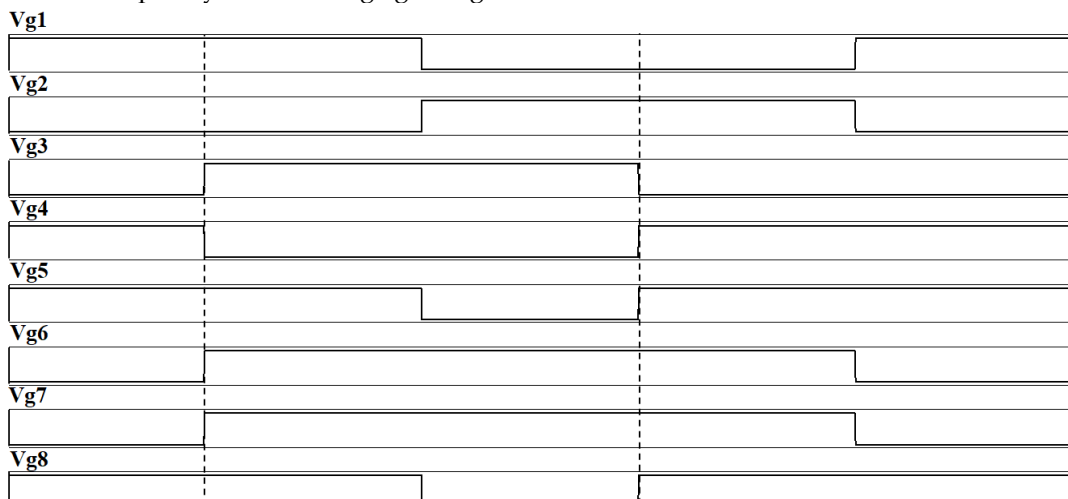
$$I_{L2,av} = \frac{2 \frac{m}{n} DV_1 - V_2}{R_{eq} + \left(2 \frac{m}{n} D\right)^2 R_{bosc}} = I_2 \tag{3}$$

152 where  $R_{eq}$  refers to all the resistive losses in the converter.

153 3.2. *Modulation strategies*

154 In Figure 5 the gate signals in the case of the previously described Phase Shift Modulation  
 155 (PSM) are shown in simulation.

156 As expected by the modulation law and highlighted by the figure, each LSbridge gate signal  
 157 event is contemporary to a HSbridge gate signal event.

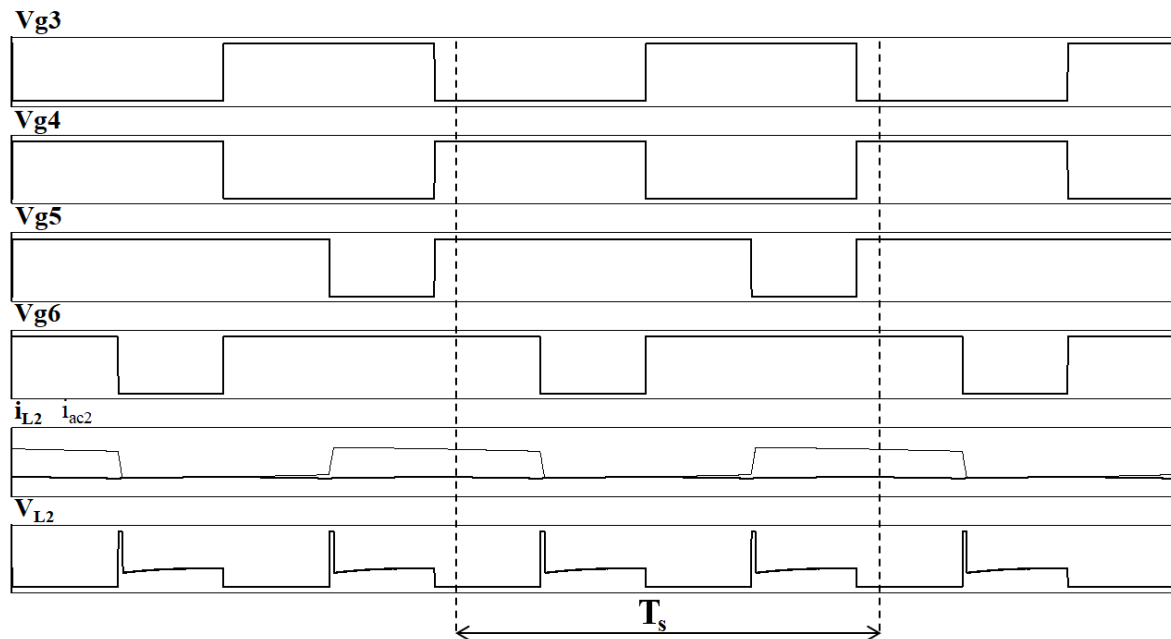


158  
 159 **Figure 5.** Gate signals in conventional PSM.

160 In Figure 6 the resulting secondary-side waveforms are highlighted, where  $V_{L2}$  is the voltage at  
 161 the output of the LSbridge and  $T_s$  is the switching period.

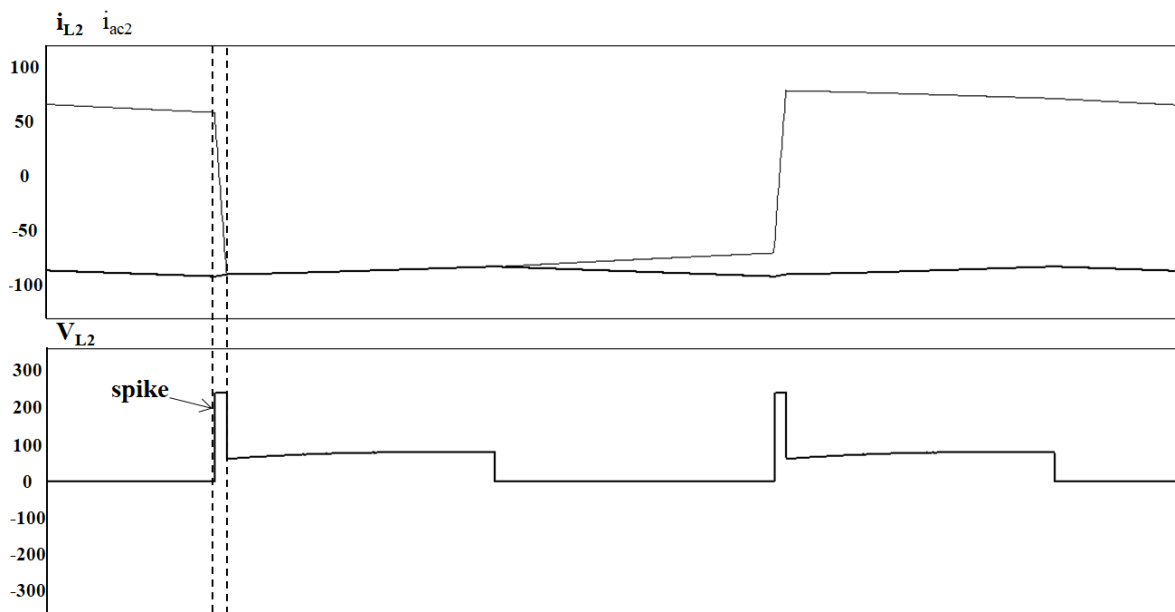
162 The considered case concerns the SOSC recharge, that is when  $I_2$  is negative, and  $I_{L2,av}$  as well. In  
 163 this case,  $I_{L2}$  is divided into the drain-source currents of M5 and M7. Every  $T_s/2$ , whenever  $V_{g5}$ - $V_{g8}$   
 164 or  $V_{g6}$ - $V_{g7}$  goes low, that is when M5 or M7 is opened, there is no conduction path through the  
 165 opened MOSFET, due to the reverse direction of the MOSFET-connected diode. Therefore, if before  
 166 the switch opening the drain-source current on the other switch was negative, a voltage spike on  $V_{L2}$   
 167 is provoked since the inductor energy is not free to circulate. This is better highlighted in Figure 7.

168 A useless energy waste is therefore shown in case of energy flow from  $V_2$  to  $V_1$  with the  
 169 conventional PSM.



170  
 171

Figure 6. Secondary-side waveforms for the conventional PSM.

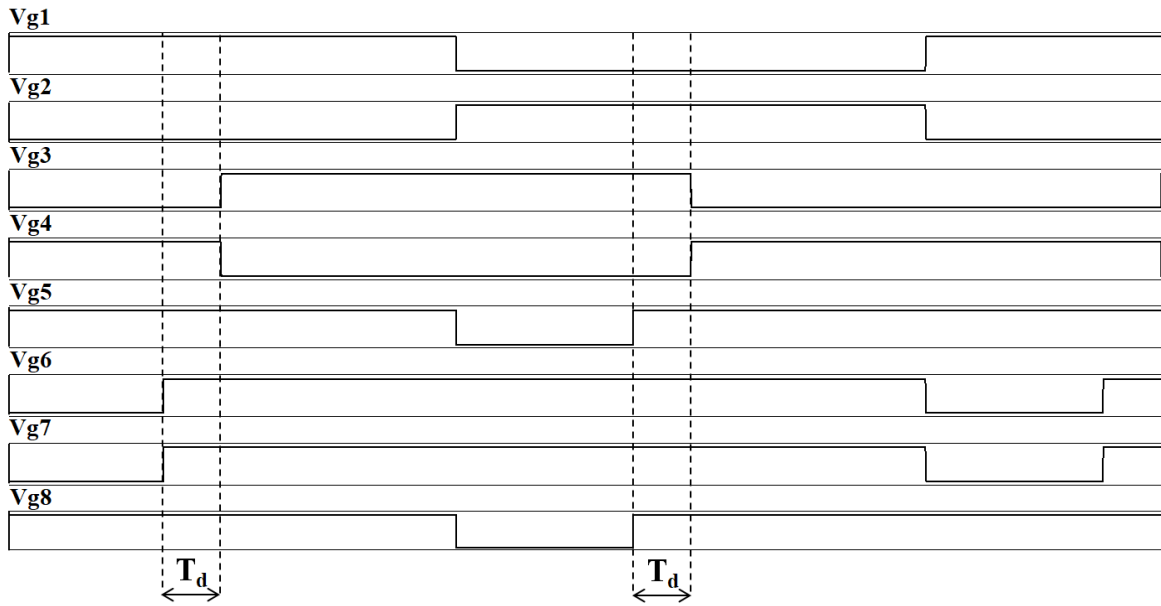


172  
 173

Figure 7. Zoom on the secondary-side waveforms for the conventional PSM.

174 In order to avoid the mentioned voltage spikes, thus avoiding to limit the overall power system  
 175 efficiency or to add an expensive clamping network, an improved modulation strategy is proposed  
 176 in the following.

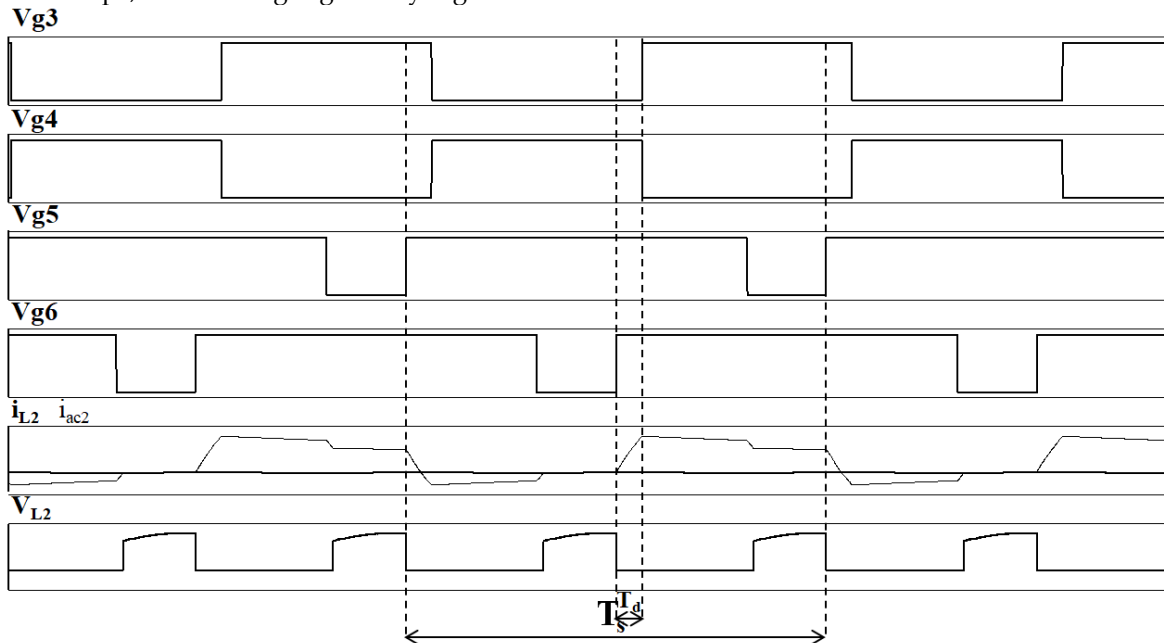
177 In Figure 8 the gate signals concerning the proposed modified Phase Shift Modulation (PSM)  
 178 are shown in simulation.



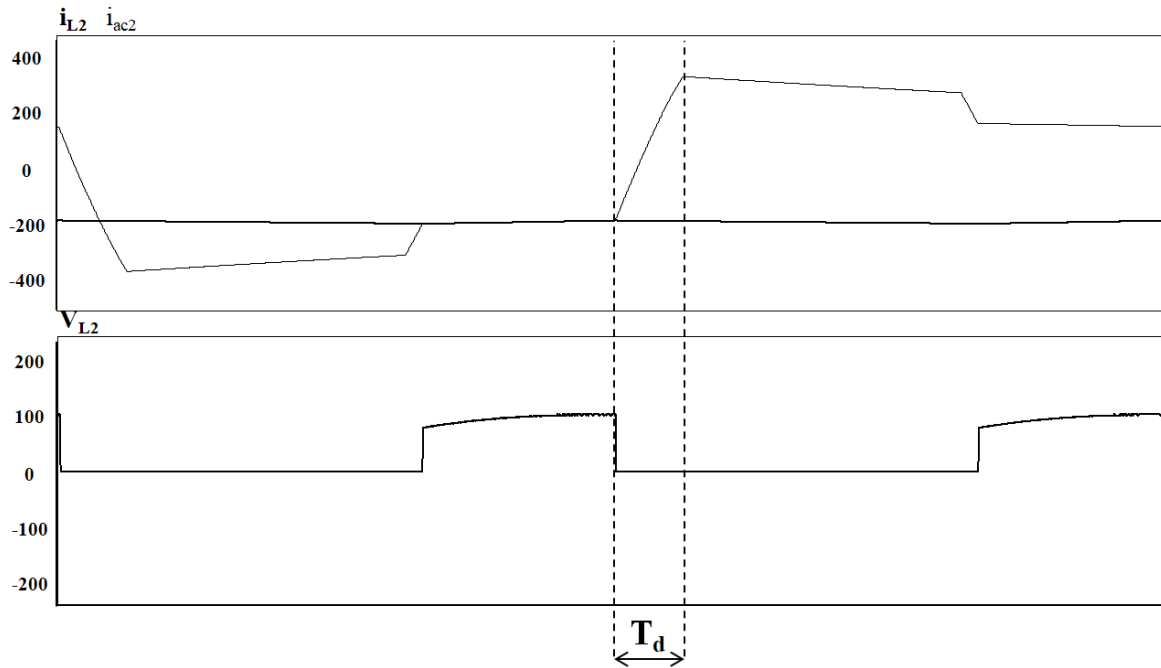
179  
 180 **Figure 8.** Gate signals in modified PSM.

181 The aim of the improved control law is to open M5-M8 (M6-M7) when the drain-source current  
 182 on M6-M7 (M5-M8) is positive (negative), that is when  $i_{ac2}$  is positive (negative). In order to reach this  
 183 goal, the positive events of  $V_{gn}$  concerning the LSbridge are anticipated by a time window,  
 184 referenced as  $T_d$ , so that  $i_{ac2}$  has the time to reverse its sign.

185 In Figure 9 the resulting secondary-side waveforms are highlighted: this time  $V_{L2}$  presents the  
 186 ideal shape, as better highlighted by Figure 10.



187  
 188 **Figure 9.** Improved secondary-side waveforms for the modified PSM.



189

190

**Figure 10.** Zoom on the secondary-side waveforms for the modified PSM.

191

A power efficiency increase is therefore achievable by means of this improved modulation strategy.

192

193

#### 4. Experimental tests

194

A FBC has been realized aiming at a 2 kW power target and compliant with the specifications concerning the DC voltage sources and the current requirements. The mounted converter consists of the following parts: the power board, including the actual FBC, filtering networks, protection switches and transducers for telemetries; a control board, including signal conditioning, input/output interfaces, controller and gate signals generation; an auxiliary power supply, including power converters to generate all internal supply lines; a mechanical frame/heatsink for thermal dissipation.

195

196

197

198

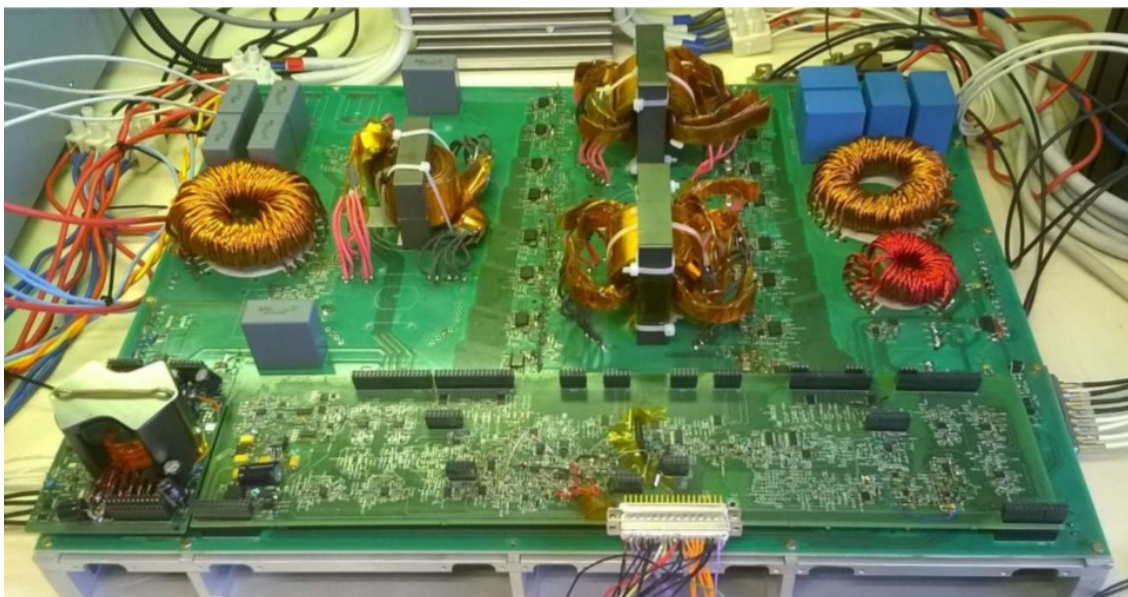
199

200

201

In Figure 11 the prototypal breadboard is shown. Auxiliary power supply board and control board on the bottom-left corner and bottom-right position can be noted.

202



203

204

**Figure 11.** The prototype of the bidirectional FBC, as built and mounted.

#### 205 4.1. H-bridges realization

206 Each power switch in the Power board consists of four parallel MOSFETs. The selected  
 207 components are compliant with Automotive applications and show a TO-247 package. Thru hole  
 208 type was found convenient as it natively provide connection to multiple PCB layers. In the  
 209 SOSC-side, AUIRFP4568 nMOSFETs have been used, rated for a maximum 171 A drain current  $I_{d,max}$   
 210 and for a maximum 150 V source-to-drain voltage  $V_{DSS}$ , with a maximum 5.9 m $\Omega$  on resistance; in the  
 211 bus-side, IXFH140N20X3 nMOSFETs have been used, rated for a maximum 140 A drain current  $I_{d,max}$   
 212 and for a maximum 200 V source-to-drain voltage  $V_{DSS}$ , with a maximum 9.6 m $\Omega$  on resistance.

213 The bus-side switches have been selected with a higher maximum voltage due to the  
 214 transformer ratio of the secondary side (bus-side) turns to the primary side (SOSC-side) turns, which  
 215 is higher than one.

216 All MOSFETs are driven by means of isolated gate drivers, useful to maintain galvanic  
 217 insulation between controller and power circuits. The selected component is UCC21521, providing  
 218 dual independent channels, useful to manage the low-side and the high-side MOSFETs, and  
 219 guaranteeing a 4-6 A (source/sink) current capability and a 16 ns time rise on a 2 nF load capacitance.

#### 220 4.2. Reactive components realization

221 As far as the used capacitors are concerned, Multi Layer Ceramic Capacitances (MLCC) are  
 222 preferred to provide the highest frequencies current peaks, since MLCC present equivalent  
 223 impedances with higher cut frequencies with respect to the electrolytic and Metallized Polyester  
 224 (PET) ones, which instead contribute to the rms component of the pulsed currents.

225 The magnetic components with pulsed currents in the tens of A range (the converter inductor  $L_2$   
 226 and the transformer) have been implemented with EE-type-cores. For the transformer, two magnetic  
 227 structures have been used, as highlighted by the figure. Copper foils have been used for the  
 228 windings and multiple wires for the connections with the PCB, in order to have a large current  
 229 capability. The material used for the transformer cores is 3C95, a power ferrite with high saturation  
 230 levels and low losses. For  $L_2$  a powder core with distributed air gap is used, whose material is *Kool*  
 231  $M\mu^{\text{®}}$  40 from *Magnetics*.

232 In Tables 3 and 4 the main characteristics of the designed and realized transformer and  $L_2$  are  
 233 respectively reported.

234 **Table 3.** Characteristics of the realized transformer.

Core	Material	n	m	Measured $L_m$	Measured $L_1$
EE80/38/20	3C95	4	6	60 $\mu$ H	140 nH

235

236 **Table 4.** Characteristics of the realized inductor.

Core	Material	Turns	Measured $L_2$
00K7228E040	Kool $M\mu^{\text{®}}$ 40	13.5	24 $\mu$ H

237

238 In Table 5 the values of the selected converter switching frequency  $f_{sw}$  and reactive  
 239 components are reported.

240 For filtering inductors, with DC currents and small ripple, toroidal powder cores are used, with  
 241 multi-wire windings. The used toroidal core materials are MolyPermalloy Powder (MPP) and High  
 242 Flux from *Magnetics*.

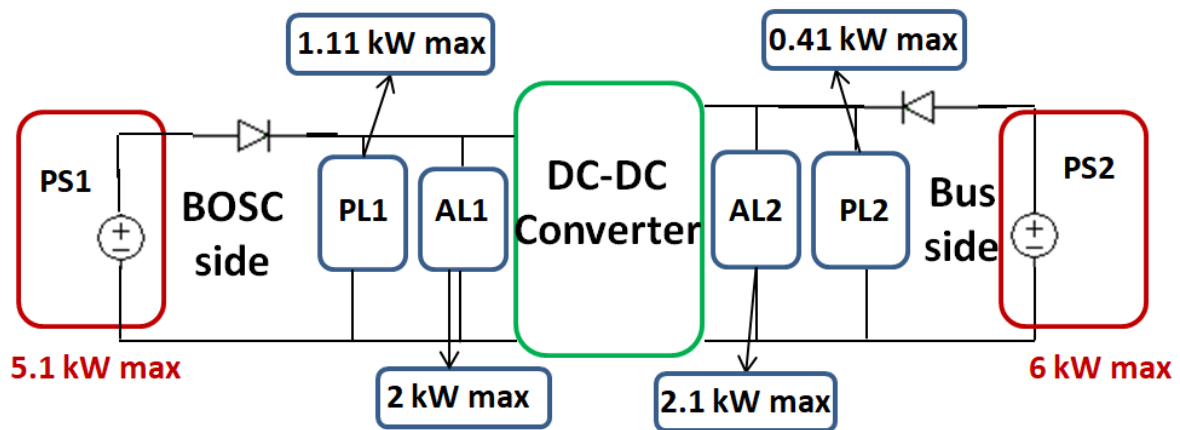
243

244 **Table 5.** Selected values of switching frequency and reactive components for the designed converter.

Parameter	Value
$f_{sw}$	50 kHz
$L_2$	24 $\mu$ H
$C_1$	130 $\mu$ F
$C_2$	200 $\mu$ H

245 4.3. Experimental setup

246 A schematic of the test setup, proposed for full power (2kW) transfer, is shown in Figure 12.



247

248 **Figure 12.** Schematic of the test setup.

249 Each side (SOSC or bus) is emulated by a 1Q (One Quadrant) Power Supply Stack – PS1 and  
 250 PS2 for SOSC and bus respectively - and a Load Stack, so that a bi-directional power flow can be  
 251 tested: when the power flows from the SOSC to the bus, PS1 provides the required energy to the  
 252 bus-side Load Stack; when the power flows from the bus to the SOSC, the SOSC-side Load Stack  
 253 adsorbs energy arising from PS2.

254 In order to avoid that a negative current flows through the power supplies, a protection diode is  
 255 used between the supply and the load. Therefore, 2 protection diodes are used, one on the SOSC side  
 256 and one on the bus side. Each of them is able to withstand a maximum 200A current, considering  
 257 that a maximum 70A current is supposed to flow in the converter and a maximum 80A current is  
 258 needed to continuously supply the Passive Loads. Therefore, in order to guarantee that both the  
 259 protection diodes are continuously polarized in direct way, a minimum direct current (supposed to  
 260 be equal to 5A) shall flow through each of them. Some Passive Loads are needed for this purpose,  
 261 in order to guarantee the required power absorption.

262 4.3.1. SOSC-side setup

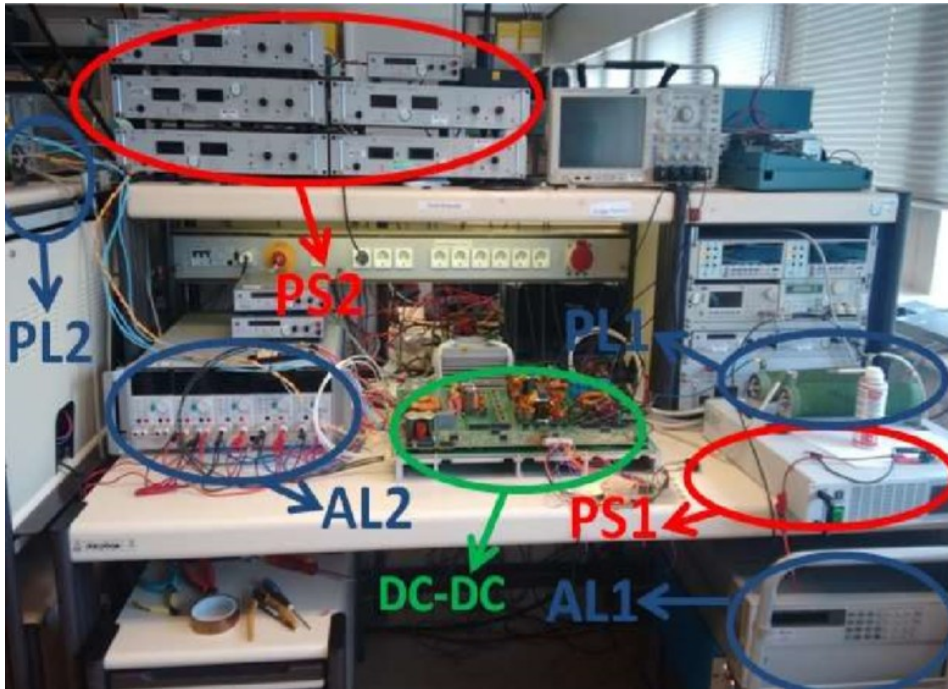
263 The goal of the SOSC test setup is to guarantee: (35V – 70V) voltage range; (-2kW - +2kW) power  
 264 range. The SOSC-side Power Supply (PS1) Stack can provide a total maximum power of 5.1 kW. The  
 265 SOSC-side Load Stack consists of an Active Load (AL1) and a Passive Load (PL1), for a total  
 266 maximum power of 3.11 kW.

267 4.3.2. Bus-side setup

268 The goal of the bus test setup is to guarantee: (24V – 32V) voltage range; (-2kW - +2kW) power  
 269 range. The bus-side Power Supply (PS2) Stack can provide a total maximum power of 6 kW. max  
 270 The bus-side Load Stack consists of an Active Load (AL2) and a Passive Load (PL2), for a total  
 271 maximum power of 2.51 kW.

272 4.4. Experimental results

273 In Figure 13 a picture of the arranged test setup is shown, along with the highlighted parts.



274

275

**Figure 13.** The arranged test setup.

276

277

278

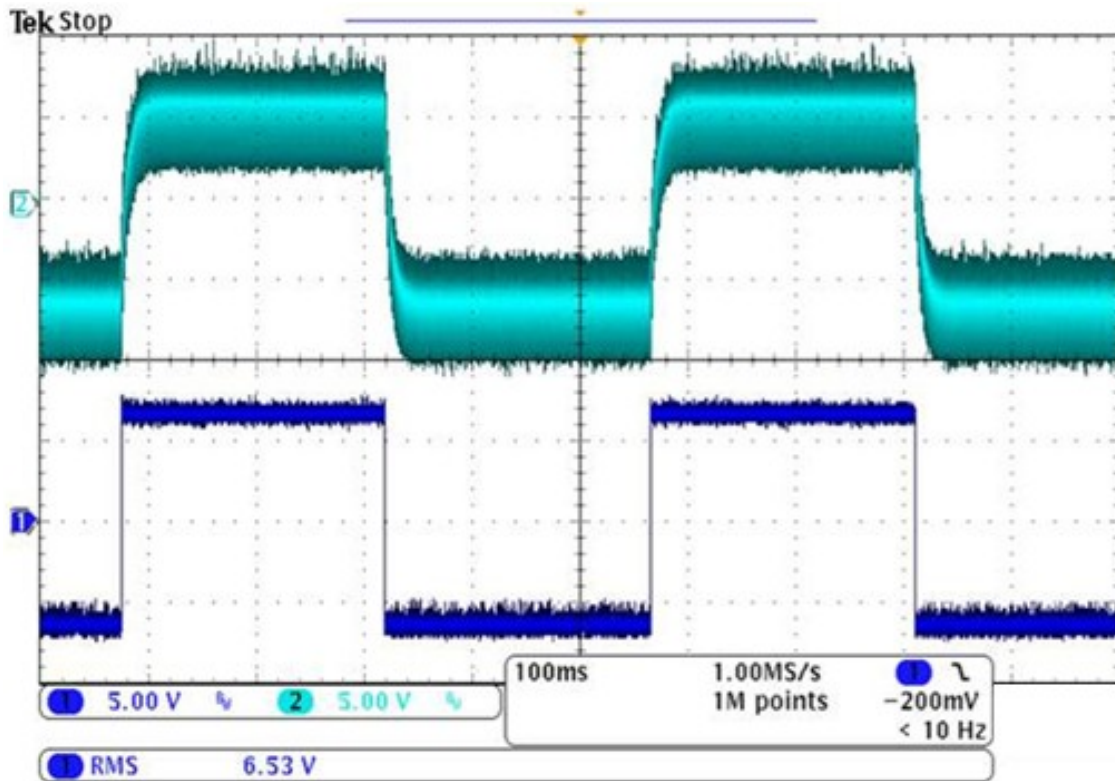
279

280

281

282

The improved PSM has been implemented for the built prototype. The proper behaviour of the converter is shown by Figure 14, showing the proper bus current response to a square wave command. The transduction factor in the command and monitoring signals is equal to 1V/10% of full power, where “full power” corresponds to a 70A bus current. Therefore, the image refers to a step between two levels corresponding to about 70% of the full negative power (during the SOSC recharge) and of the full positive power (during the SOSC discharge). There are no overshoot phenomena in the transients.



283

284

285

286

**Figure 14.** The proposed behaviour of the bus current (in light blue), as experimentally tested, corresponding to a given power profile (in blue). For the monitoring signal (light blues) and the command signal (blue) 1 V is equivalent to the 10% of the full power.

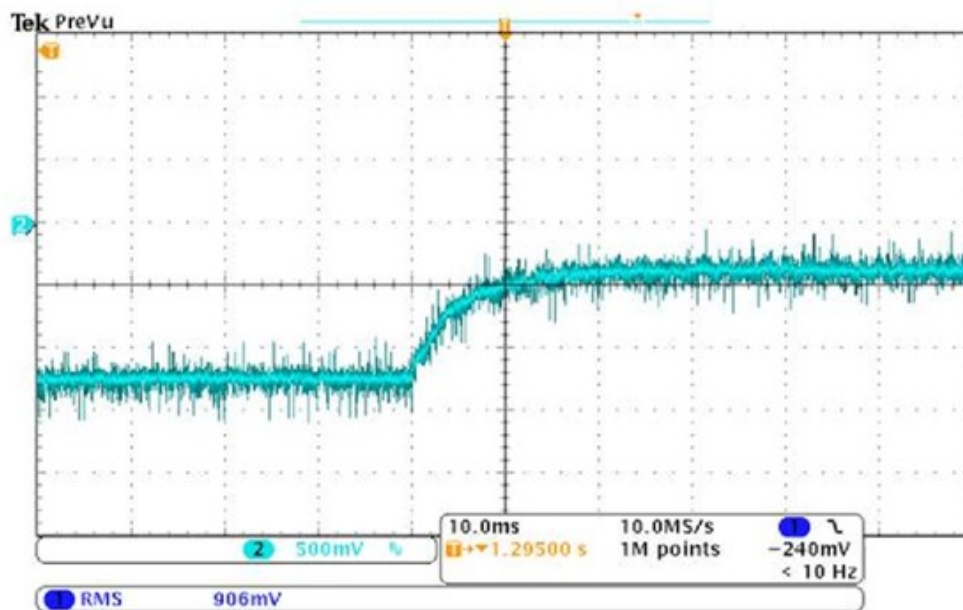
287

288

289

290

Figures 15 and 16 show a zoom of the positive and negative transients respectively. Response time is compliant with the requirements, according to typical applications where 100 ms maximum response times are allowed. A further improvement of the response time is possible through a slight refinement of the control loop

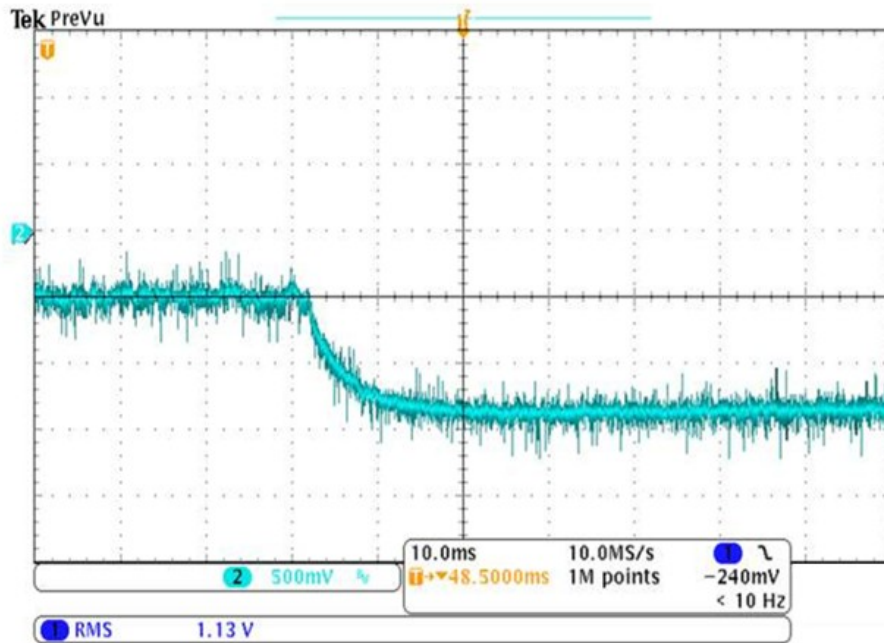


291

292

293

**Figure 15.** Zoom on a positive bus current transient, responding to an instantaneous positive command.



294

295 **Figure 16.** Zoom on a negative bus current transient, responding to an instantaneous negative  
 296 command.

## 297 5. Conclusions

298 In this paper, an insulated bidirectional DC-DC converter for the management of a storage  
 299 system is proposed. Electrical Storage Systems find different possible application fields: automotive,  
 300 zero-energy buildings, aerospace, etc. The described topology is a Full-Bridge Converter (FBC),  
 301 connected to a double voltage source: a voltage bus on one side and a Stack Of Super-Capacitors  
 302 (SOSC) on the other side. Analysis, design and modulation strategies of the proposed FBC are  
 303 discussed. An improved modulation strategy has been proposed by authors, aiming at avoiding  
 304 expensive clamping networks and at the power losses reduction. A 2 kW converter prototype,  
 305 including also control and auxiliary power supply boards and compliant with automotive  
 306 applications, has been realized, and the related experimental results have been presented as well,  
 307 proving the proper behaviour of the converter.

308 **Author Contributions:** Authors contributed equally to the presented work.

309 **Funding:** This work was financially supported by: MIUR-Ministero dell'Istruzione, dell'Università e della  
 310 Ricerca (Italian Ministry of Education, University and Research), PON R&I 2014-2020 - AIM (Attraction and  
 311 International Mobility), project AIM1851228-1; AEROSPOWER Lab (Aerospace Power Laboratory) of Scuola di  
 312 Ingegneria Aerospaziale, "Sapienza" University of Rome; ESA (European Space Agency), Contract No.  
 313 4000116941/16/NL/MH; Airbus Safran Launchers SAS; PON R&I 2015-2020 PROPulsione e Sistemi IBridi per  
 314 velivoli ad ala fissa e rotante PROSIB, CUP no:B66C18000290005; PRIN 2017, Advanced power-trains and  
 315 -systems for full electric aircrafts, prot. no.: 2017MS9F49; project REACTION (first and euRopEAn siC eight  
 316 Inches pilOt liNe), co-funded by the ECSEL Joint Undertaking under grant agreement No 783158; SDESLab  
 317 (Sustainable Development and Energy Saving Laboratory) of University of Palermo; RPLab (Rapid Prototyping  
 318 Laboratory - University of Palermo); LEAP (Laboratory of Electrical Applications) of University of Palermo.

319 **Conflicts of Interest:** The authors declare no conflict of interest.

320

321 **References**

- 322 1. Livreri, P.; Caruso, M.; Castiglia V.; Pellitteri, F.; Schettino, G. Dynamic reconfiguration of electrical  
323 connections for partially shaded PV modules: Technical and economical performances of an  
324 Arduino-based prototype. *Int. J. Renew. Energy Res.* **2018**, *8*(1), 336-344.
- 325 2. Di Carlo, C. A.; Di Donato, L.; Mauro, G. S.; La Rosa, R.; Livreri, P.; Sorbello, G. A circularly polarized  
326 wideband high gain patch antenna for wireless power transfer. *Microw. Opt. Techn. Let.* **2018**, *60*(3),  
327 620-625.
- 328 3. La Rosa, R.; Zoppi, G.; Finocchiaro, A.; Papotto, G.; Di Donato, L.; Sorbello, G.; Bellomo, F.; Di Carlo C. A.;  
329 Livreri, P. An over-the-distance wireless battery charger based on RF energy harvesting. In Proceedings of  
330 the 14th International Conference on Synthesis, Modeling, Analysis and Simulation Methods and  
331 Applications to Circuit Design (SMACD), IEEE, 2017, pp. 1-4.
- 332 4. Yoo, H.; Sul, S.-K.; Park, Y.; Jeong, J. System integration and power-flow management for a series hybrid  
333 electric vehicle using supercapacitors and batteries. *IEEE Trans. Ind Appl.* **2008**, *44* (1), 108-114.
- 334 5. Abdelhedi, R.; Chiheb Ammari, A.; Sari, A.; Lahyani, A.; Venet, P. Optimal power sharing between  
335 batteries and supercapacitors in Electric vehicles. In Proceedings of the 7th International Conference on  
336 Sciences of Electronics, Technologies of Information and Telecommunications (SETIT), 2016, pp. 97-103.
- 337 6. Angerer, C.; Krapf, S.; Wassiliadis, N.; Lienkamp, M.; Reduction of aging-effects by supporting a  
338 conventional battery pack with ultracapacitors. In Proceedings of the Twelfth International Conference on  
339 Ecological Vehicles and Renewable Energies (EVER), IEEE, 2017, pp. 1-12.
- 340 7. Shah, N.; Czarkowski, D. Supercapacitors in Tandem with Batteries to Prolong the Range of UGV Systems.  
341 *Electronics* **2018**, *7*(1), 6, 1-12.
- 342 8. Zhang, Q.; Li, G. Experimental Study on a Semi-Active Battery-Supercapacitor Hybrid Energy Storage  
343 System for Electric Vehicle Application. *IEEE Trans. Power Electron.* **2019**, *35*(1), 1014-1021.
- 344 9. Yaïci, W.; Kouchachvili, L.; Entchev, E.; Longo, M. Dynamic Simulation of Battery/Supercapacitor Hybrid  
345 Energy Storage System for the Electric Vehicles. In Proceedings of the International Conference on  
346 Renewable Energy Research and Applications (ICRERA), IEEE, 2019, pp. 460-465.
- 347 10. Pellitteri, F.; Castiglia, V.; Livreri, P.; Miceli, R. Analysis and design of bi-directional DC-DC converters for  
348 ultracapacitors management in EVs. In Proceedings of the International Conference on Ecological Vehicles  
349 and Renewable Energies (EVER), IEEE, 2018, pp. 1-6.
- 350 11. Livreri, P.; Castiglia, V.; Pellitteri, F.; Miceli, R. Design of a Battery/Ultracapacitor Energy Storage System  
351 for Electric Vehicle Applications. In Proceedings of the 4th International Forum on Research and  
352 Technologies for Society and Industry (RTSI), IEEE, 2018, pp. 1-5.
- 353 12. Castiglia, V.; Livreri, P.; Miceli, R.; Pellitteri, F.; Schettino, G.; Viola, F. Power Management of a  
354 Battery/Supercapacitor System for E-Mobility Applications. In Proceedings of the AEIT International  
355 Conference of Electrical and Electronic Technologies for Automotive (AEIT AUTOMOTIVE), IEEE, 2019,  
356 pp. 1-5.
- 357 13. Chakraborty, S.; Vu, H. N.; Hasan, M. M.; Tran, D. D.; Baghdadi, M. E.; Hegazy, O. DC-DC Converter  
358 Topologies for Electric Vehicles, Plug-in Hybrid Electric Vehicles and Fast Charging Stations: State of the  
359 Art and Future Trends. *Energies* **2019**, *12*(8), 1569, 1-43.
- 360 14. Karbozov, A.; Ibanez, F. M. Optimal Design Methodology for High-Power Interleaved Bidirectional  
361 Buck-Boost Converters for Supercapacitors in Vehicular Applications. In Proceedings of the 8th  
362 International Conference on Renewable Energy Research and Applications (ICRERA), IEEE, 2019, pp.  
363 152-157.
- 364 15. Sadoun, R.; Rizoug, N.; Bartholomeus, P.; Barbedette, B.; LeMoigne, P. Sizing of hybrid supply  
365 (battery-supercapacitor) for electric vehicle taking into account the weight of the additional buck-boost  
366 chopper. In Proceedings of the First International Conference on Renewable Energies and Vehicular  
367 Technology, IEEE, 2012, pp. 8-14.
- 368 16. Camara, M. B.; Gualous, H.; Gustin, F.; Berthon, A. Design and new control of DC/DC converters to share  
369 energy between supercapacitors and batteries in hybrid vehicles. *IEEE Trans. Veh. Technol.* **2013**, *57*(5),  
370 2721-2735.
- 371 17. Xue, L. K.; Wang, P.; Wang, Y. F.; Bei, T. Z.; Yan, H. Y. A four-phase high voltage conversion ratio  
372 bidirectional DC-DC converter for battery applications. *Energies* **2015**, *8*(7), 6399-6426.

- 373 18. Zhang, H.; Chen, Y.; Park, S. J.; Kim, D. H. A Family of Bidirectional DC–DC Converters for Battery  
374 Storage System with High Voltage Gain. *Energies* **2019**, *12*(7), 1289, 1-21.
- 375 19. Lai, C. M. Development of a novel bidirectional DC/DC converter topology with high voltage conversion  
376 ratio for electric vehicles and DC-microgrids. *Energies* **2016**, *9*(6), 410, 1-25.
- 377 20. Ikeda, S.; Kajiwara, K.; Tsuji, K.; Kurokawa, F. Efficiency improvement of isolated bidirectional boost full  
378 bridge dc-dc converter. In Proceedings of the 7th International Conference on Renewable Energy Research  
379 and Applications (ICRERA), IEEE, 2019, pp. 673-676.
- 380 21. Lee, I. O.; Lee, J. Y. A High-Power DC-DC Converter Topology for Battery Charging Applications. *Energies*  
381 **2017**, *10*(7), 871, 2-17.
- 382 22. Shen, C. L.; Shen, Y. S.; Tsai, C. T. Isolated DC-DC Converter for Bidirectional Power Flow Controlling  
383 with Soft-Switching Feature and High Step-Up/Down Voltage Conversion. *Energies* **2017**, *10*(3), 296, 1-23.
- 384 23. Pellitteri, F.; Boscaino, V.; Di Tommaso, A. O.; Miceli, R.; Capponi, G. Experimental test on a Contactless  
385 Power Transfer system. In Proceedings of the Ninth International Conference on Ecological Vehicles and  
386 Renewable Energies (EVER), IEEE, 2014, pp. 1-6.
- 387 24. Inoue, S.; Akagi, H. A bidirectional DC–DC converter for an energy storage system with galvanic isolation.  
388 *IEEE Trans. Power Electron.* **2007**, *22*(6), 2299-2306.
- 389 25. Pellitteri, F.; Caruso, M.; Castiglia, V.; Di Tommaso, A. O.; Miceli, R.; Schirone, L. An inductive charger for  
390 automotive applications. In Proceedings of the 42nd Annual Conference of the IEEE Industrial Electronics  
391 Society (IECON), IEEE, 2016, pp. 4482-4486
- 392 26. Caruso, M.; Castiglia, V.; Di Tommaso, A. O.; Miceli, R.; Pellitteri, F.; Schirone, L. Efficient contactless  
393 power transfer system for EVs. In Proceedings of the 51st International Universities Power Engineering  
394 Conference (UPEC), IEEE, 2016, pp. 1-6.
- 395 27. Pellitteri, F.; Boscaino, V.; Di Tommaso, A. O.; Miceli, R.; Capponi, G. Control subsystem design for  
396 wireless power transfer. In Proceedings of the International Conference on Renewable Energy Research  
397 and Application (ICRERA), IEEE, 2014, pp. 980-984.



© 2020 by the authors. Submitted for possible open access publication under the terms and conditions of the Creative Commons Attribution (CC BY) license (<http://creativecommons.org/licenses/by/4.0/>).